



Kinetics and mechanistic study on deoxygenation of pyridine oxide catalyzed by {MeRe^VO(pdt)}₂ dimer



Abdellatif Ibdah*, Salwa Alduwikat

Department of Chemistry, Jordan University of Science and Technology, Irbid, Jordan

ARTICLE INFO

Article history:

Received 27 February 2017

Received in revised form

26 April 2017

Accepted 28 April 2017

Available online 3 May 2017

Keywords:

Oxygen atom transfer

DFT

Kinetics

ABSTRACT

The oxorhenium(V) dimer {MeReO(pdt)}₂ (where pdt = 1,2-propanedithiolate) catalyze the oxygen atom transfer (OAT) reaction from the pyridine oxide to triphenylarsine (Ph₃As). The rate law is given by $v = k [Re\text{-dimer}][PyNO]$ and zero order dependence on Ph₃As. The value of k at 25 °C in CHCl₃ is $139 \pm 3 \text{ L mol}^{-1} \text{ s}^{-1}$. The activation parameters are $\Delta H^\ddagger = 12.2 \pm 1.0 \text{ kcal mol}^{-1}$ and $\Delta S^\ddagger = -7.9 \pm 3.24 \text{ cal K}^{-1} \text{ mol}^{-1}$. According to the proposed mechanism, the rate determining step is the oxidation of Re^VO to Re^{VII}O₂ and the pyridine release. The triphenylarsine enters the catalytic cycle after the rate determining step. The reaction constant $\rho = -1.4$ obtained from Hammett correlation with σ for different substituted pyridine N-oxide. The computational study indicates that the oxidation of Re^V to Re^{VII} and release of the pyridine step is insensitive to the nature of the substituent on the pyridine with the average estimated activation barrier ≈ 11.5 kcal/mol from six different substituted pyridine oxide. It is proposed that electron donor substituent enrich the equilibrium of the first step of the proposed mechanism which is the coordination of the pyridine oxide with one rhenium atom to form I₁ (Scheme 2). The electron donor substituent on the pyridine increase the concentration of I₁ which will increase the rate of the reaction as the $v = k_2[I_1]$.

© 2017 Elsevier B.V. All rights reserved.

1. Introduction

Since decades, the oxygen atom transfer reaction (OAT) catalyzed by high valent oxo transition metal complexes have been attracted the scientific attention due to its application in biology [1] and chemistry [2–4]. In biology, molybdenum and tungsten are exist in the active-site of certain enzymes. These enzymes catalyze the oxygen atom transfer reaction and often called oxotransferase enzyme. Their catalytic cycle runs between M^(VI)O₂ and M^(IV)=O (M = Mo, W) [1]. In chemistry, alkene oxidation, sulfide oxidation to sulfoxide, and deoxygenation of pyridine oxide through OAT reactions are extensively employed in a wide range of areas of preparative organic chemistry. Considering the interest in developing an efficient catalysis for oxygen atom transfer reaction (OAT), several transition metal complexes have synthesized and their catalytic activity have been examined. Most of these complexes have metal oxo (M = O) bond in their structures like molybdenum, tungsten [4,5], iron [2], manganese [6,7], and rhenium [8,9].

The mechanistic studies of oxygen atom transfer catalyzed by transition metal complexes have been studied as an essential step in preparing a more efficient catalysis. In addition to experiments, several computational studies have been employed into the high valent transition metal oxo complexes [6,8,10,11]. The proposed catalytic cycle begins with oxidation of Mⁿ=O by an oxygen donor to produce Mⁿ⁺²O₂ followed by reduction of Mⁿ⁺²O₂ back to Mⁿ=O by an oxygen acceptor [1,4,5]. The Re^V=O/Re^{VII}O₂ system can be constructed to be used as catalysis for oxygen atom transfer. Several dithiolate Re^V=O complexes has been prepared and their catalytic activity has been examined [9,12–26]. The high valent rhenium(V) oxo complexes have shown a great ability to catalyze the oxidation reaction [16,20–28].

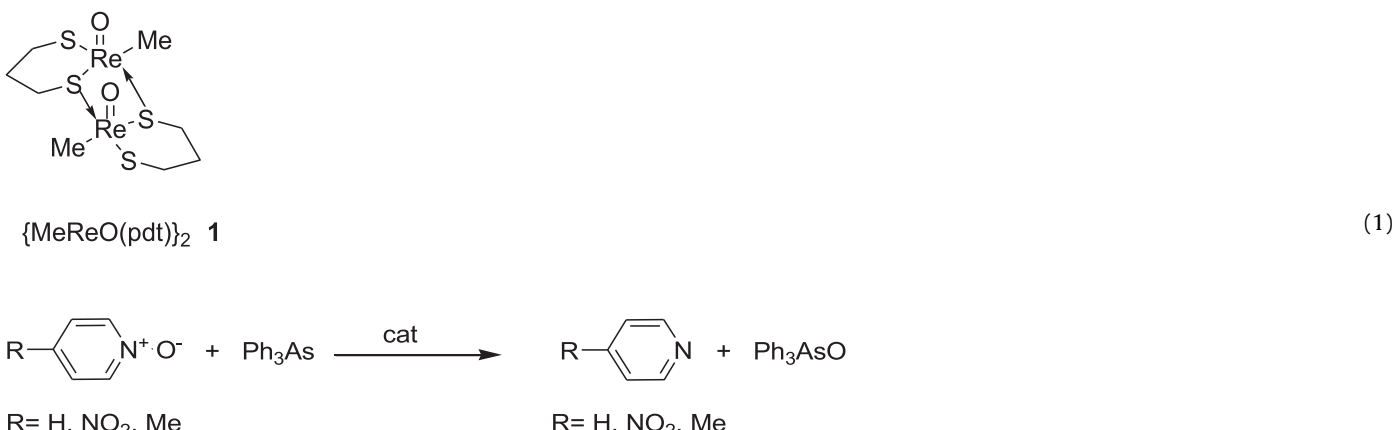
The deoxygenation of heteroaromatic N-oxides are important as intermediate step in the heterocycles synthesis [29,30]. Many of the known methods for deprotection of pyridines are limited by the side reactions or by reduction of the ring substituents. Moreover, pyridine and other heteroarene N-oxides are important class of heteroaromatic compounds in medicinal [31] and material chemistry [32]. The development of an efficient deoxygenation method is highly desirable that can be used during the functionalization of N-heterocycles [33,34].

* Corresponding author.

E-mail address: aibdah@just.edu.jo (A. Ibdah).

The purpose of this work is to study the pyridine oxide deoxygenation catalyzed by oxorhenium dimer $\{\text{MeReO}(\text{pdt})\}_2$ (1) ($\text{pdt} = 1,3\text{-propanedithiolate}$) according to the following equation. The dimeric catalyst was chosen because, in earlier studies, dimeric systems had proved to be approximately 100 times more effective than monomeric analogues [35].

implemented in GAMESS [39,40]. All the structures were fully optimized with B3LYP using PCM solvation model of chloroform with the following basis set: the LANL2DZ ECP augmented with 2f polarization functions for Re [41] and 6-31G(d) basis sets were used for other atoms. The structures were confirmed as minima or transition states by calculating vibrational frequencies at same level



The above reaction is very important reaction to study because no uncatalyzed reaction has been observed even though it's thermodynamically favored. The As-O (102.6 kcal/mol [36]) bond dissociation energy is stronger than the bond dissociation energy of N-O (61.7 kcal/mol [37]) and the entropy change ($\Delta S \approx 0$) is expected to be very small. So, the above reaction has a negative Gibbs free energy ($\Delta G < 0$).

2. Experimental section

2.1. Reagent

The Rhenium dimer $\{\text{MeReO}(\text{pdt})_2\}$ (**1**) (pdt = 1,2-propanedithiolate) was synthesized according to the literature experimental procedure [38]. Other reagents were purchased from commercial sources and used without extra purification. The solvent used for kinetics study is chloroform. Bruker 400 MHz spectrometers used to obtain ^1H and ^{31}P NMR spectra. Benzene- d_6 was used for rhenium(V) dimer ^1H -NMR characterization to compare with literature values.

2.2. Kinetic measurements

The reactions were studied at 25 °C. Shimadzu scanning spectrophotometers (UV-2550) were used to record UV–Vis spectra and kinetic curves in cells with 1 cm optical path lengths. The reaction progress was monitored from the intensity of pyridine oxide, picoline oxide, and nitro pyridine oxide absorbance at, 307 nm, 309 nm, and 375 nm respectively. The time-absorbance data were fitted to first-order kinetics, Eq (2), in which Y = absorbance of pyridine oxide substrate.

$$Y_t = Y_\infty + (Y_0 - Y_\infty)e^{-k_{obs}t} \quad (2)$$

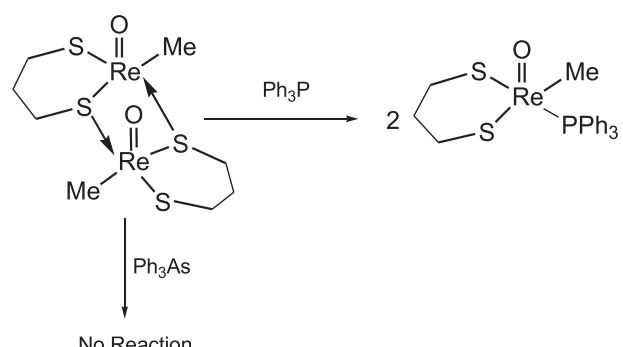
2.3. Computational methods

Computations were carried out using the DFT calculation, as

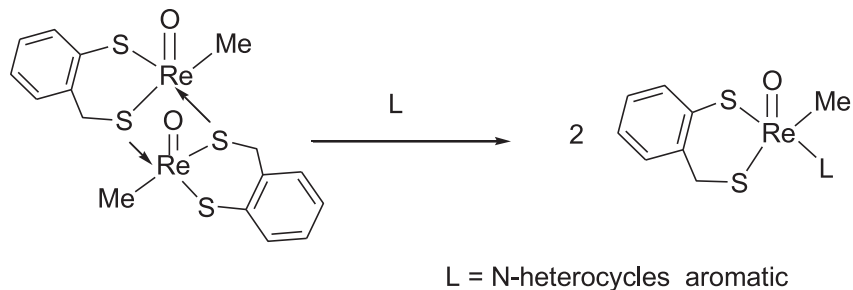
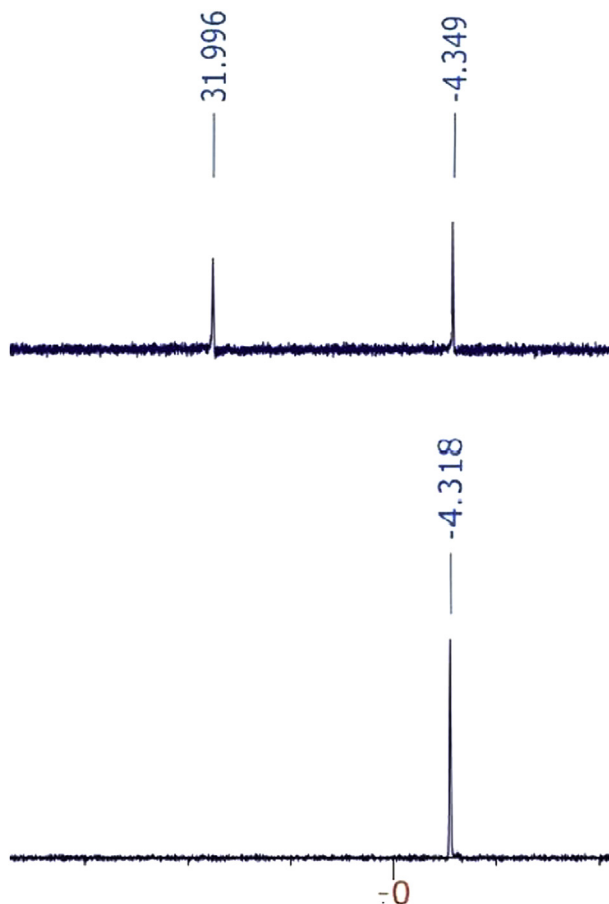
of theory and basis sets. The zero point, entropy change (ΔS°), and the temperature correction to the energy is calculated with same basis set and level of theory. Energies were refined with single point calculations on the optimized geometries using Minnesota exchange-correlation M11-L [42] with PCM solvation model of chloroform with the following basis sets: G3Large for As, 6-311(3df) for S and Cl, 6-311G(d) for O, N, C and H, along with the same basis set for Re.

3. Result and discussion

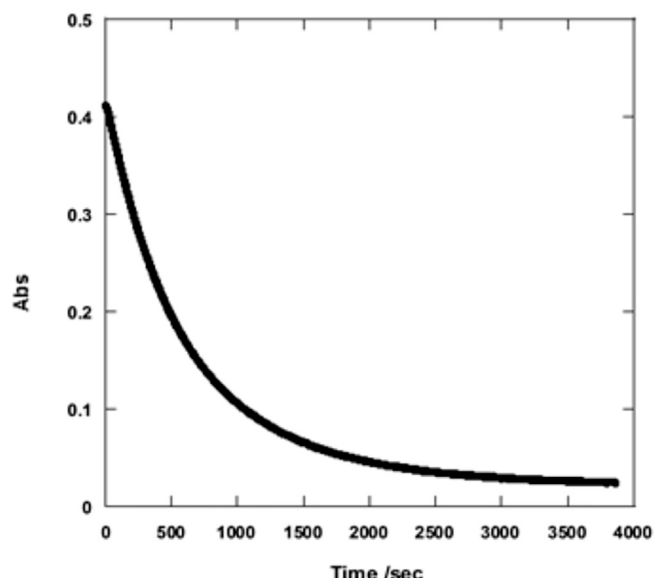
The characterization of the product has been done with Ph₃P using the ³¹P-NMR. The Ph₃P is used only for the purpose of the product characterization because the dimer reacts with phosphine to form a monomer (**Scheme 1**) and phosphine monomer is very slow comparing to dimer [35,43,44]. The catalysis 1 is stable with respect to monomerization by arsines, even over long reaction time no MeReO(pdt) (AsPh₃) monomer has not been detected. Also, the catalysis 1 is found to be stable toward monomerization with pyridine (the reaction product). This result is very important because similar rhenium dimer can be monomerized with pyridine and other *N*-heterocycles aromatic compounds (**Scheme 2**) [23,28,44–47].



Scheme 1. Monomerization reaction of $\{\text{MeReO}(\text{pdt})\}_2$ dimer occurs with phosphines.

**Scheme 2.** Monomerization reaction between dimer and *N*-heterocycles aromatic compounds.**Fig. 1.** ^{31}P -NMR spectrum before (below) and after (above) completion (2.5 h) of a reaction between 25 mM pyridine *N*-oxide, 140 mM PPh_3 , and 3.86 mM Re dimer. The resonance at 31.9 ppm in CDCl_3 is for Ph_3PO .

The Ph_3PO was the only oxide product formed from the deoxygenation reaction of pyridine oxide (Fig. 1). The rest of the kinetics measurement were made with Ph_3As as oxygen acceptor. The absorbance decrease of pyridine oxide was monitored under pseudo first order condition of Ph_3As ($[\text{Ph}_3\text{As}] \gg [\text{PyNO}]$) (Fig. 2). The absorbance decrease conformed first order dependence on the pyridine oxide concentration. The k_{obs} values obtained from the first order fitting of Eq (2) conformed zero dependent with respect to the Ph_3As concentration (Fig. 3) and has linear dependence on the rhenium dimer catalyst concentration confirming the first order dependence on rhenium dimer (Fig. 3).

**Fig. 2.** The pyridine oxide absorbance at 307 nm decrease with 0.5 mM pyridine oxide, 10.0 mM Ph_3As , and 0.01 mM catalysis.

Based on the experimental observation the rate law can be written as: $R = k[\text{PyNO}][\text{Re}][\text{Ph}_3\text{As}]^0$. $k = 139 \pm 3 \text{ M}^{-1}\text{s}^{-1}$. The first order dependence on the pyridine oxide and the rhenium catalyst imply that the rate determining step involve the pyridine oxide and the catalyst only. The zero order dependence on the Ph_3As indicates that it inter the catalytic cycle after the rate determining step.

3.1. Para-substituted pyridine-oxide

More kinetic measurements have been done with substituted pyridine oxide to compare with the pyridine oxide. The 4-nitropyridine oxide and picoline oxide (4-methyl-pyridine oxide) were the chosen substrates for the kinetic study. The absorbance decrease of the nitro-pyridine oxide and picoline oxide were observed under pseudo first order conditions of Ph_3As ($[\text{Ph}_3\text{As}] \gg [\text{nitropyridine oxide}]$ and $[\text{Ph}_3\text{As}] \gg [\text{picoline oxide}]$) (Fig. 4). Similar to PyNO reaction, the absorbance decrease confirmed a first order dependence on the 4-nitropyridine oxide and picoline oxide but the nitro substituent is slower the pyridine oxide and the methyl substituent is faster than the pyridine oxide (Fig. 4).

The calculated k_{obs} values from the first order fitting confirmed the zero order dependence on the Ph_3As and first order dependence on the rhenium catalyst for both 4-nitropyridine oxide and

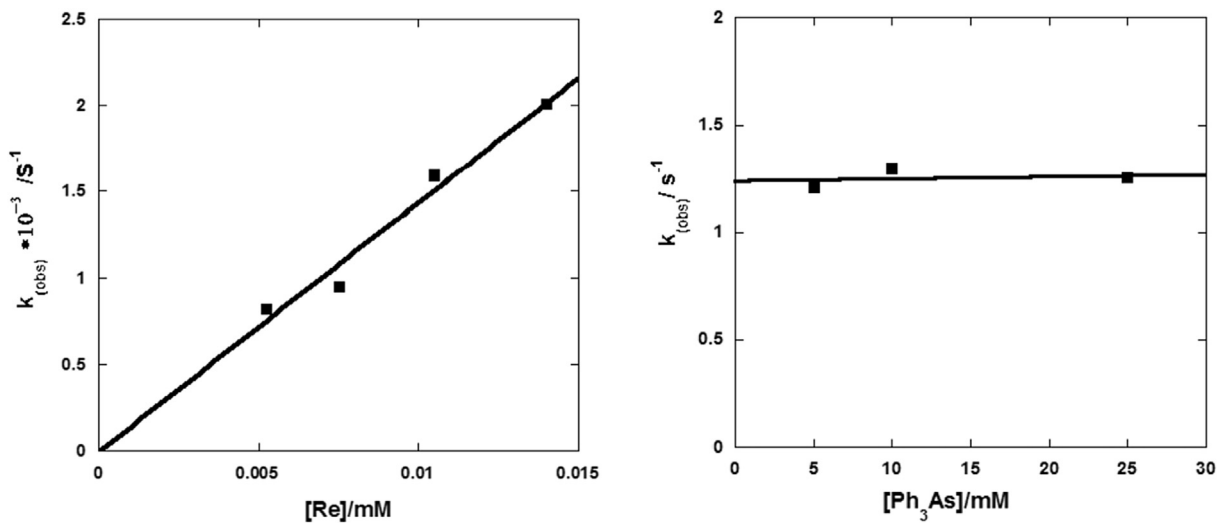


Fig. 3. (Left) Plot of k_{obs} against the Re concentration with 0.5 mM Pyridine oxide and 10.0 mM Ph_3As . (Right) Plot of k_{obs} against Ph_3As concentration with 0.5 mM pyridine oxide and 0.01 mM of Re catalyst.

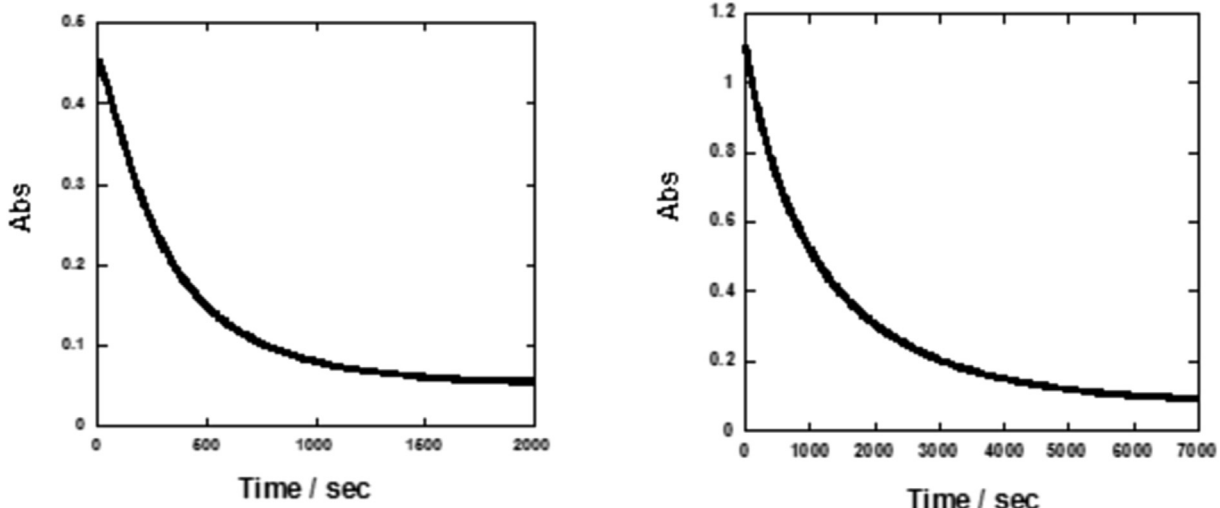


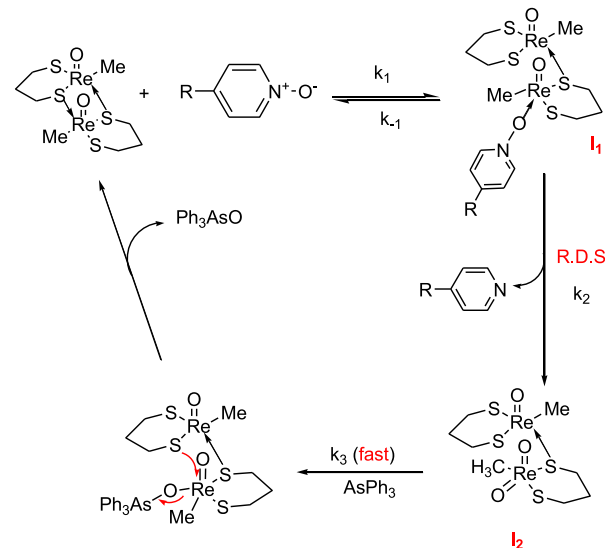
Fig. 4. (Left) The picoline oxide absorbance at 309 nm decrease with 0.38 mM picoline oxide, 10.0 mM Ph_3As , and 0.01 mM catalysis. (Right) The 4-nitropyridine oxide absorbance at 375 nm decrease with 0.25 mM 4-nitropyridine oxide, 5.0 mM Ph_3As , and 0.05 mM catalysis.

picoline oxide (see [supporting information](#)). These kinetics results are equivalent to the pyridine oxide results. Also, the first order fitting on pyridine oxide substrates retain even at low concentration of Ph_3As (less than the pseudo order conditions) which confirm the zero dependence on the arsine. The rate constant k is $16.5 \pm 0.8 \text{ M}^{-1}\text{s}^{-1}$ and $388 \pm 14 \text{ M}^{-1}\text{s}^{-1}$ for 4-nitropyridine oxide and picoline oxide, respectively.

The reaction rate became slower with electron withdrawing substituent (NO_2 substituent) on the pyridine oxide and faster with electron donor substituent (methyl substituent). The rate determining step remains same and the Ph_3As inter the catalytic cycle after the rate determining step.

3.2. Reaction scheme and the mechanism

The kinetics data allow the construction of the reaction mechanism as presented in [Scheme 3](#). The first step of the proposed mechanism is the coordination of the pyridine oxide to one rhenium atom concomitant with release one Re-S coordinate bond to form five coordinated intermediate I_1 in fast equilibrium. The following step is the irreversible release of the pyridine to form of



Scheme 3. The Proposed mechanism of the oxygen atom transfer catalyzed by $(\text{MeRe}^{\text{V}}\text{O(pdt)})_2$ dimer.

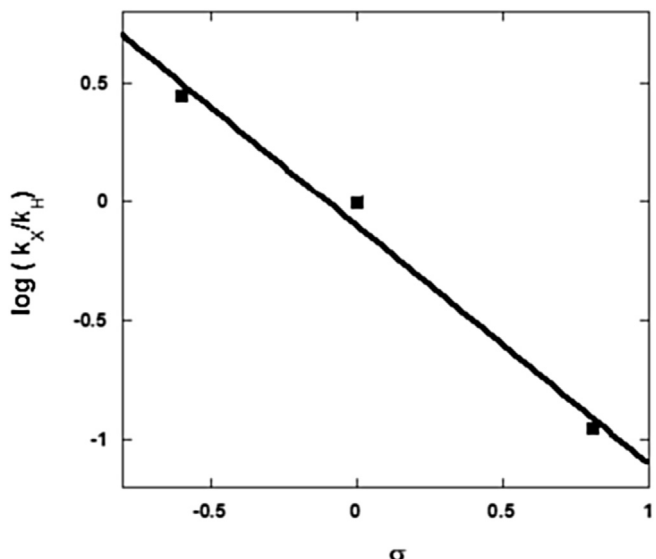


Fig. 5. The Hammett analysis of the relative rate constant of pyridine oxide substituent.

Table 1
The ratio of the rate constant (k_X/k_H) to hammett substituent content.

X-PyN-O	$k_X \text{ L mol}^{-1} \text{ s}^{-1}$	k_X/k_H	σ
NO ₂ -PyN-O	15.3	0.11	0.78
PyN-O	136.3	1.00 (rel)	0.0
Me-PyN-O	390.2	2.87	-0.17

ReO₂^(VII) intermediate I₂ and it is the rate controlling step. The Ph₃As react with the ReO₂^(VII) intermediate I₂ in fast step to reduce Re^{VII} and form Re^(V)-OAsPh₃ intermediate. Then the Re-S coordinate bond will be regenerated concomitant to release Ph₃AsO. The

catalyst will be restored to start another cycle. Analogous system of rhenium catalysts adopt similar kinetics dependence that the ReO₂^(VII) formation is the slow step followed by fast addition of the oxygen acceptor (e.g Ph₃P/Ph₃As) [44,48,49].

On the basis of **Scheme 3**, the rate expression can be derived considering prior-equilibrium in the first step (I₁ formation) followed by the R.D.S formation of I₂ (Full derivation of the rate law is in the [supporting information](#)).

$$\nu = \frac{k_1 k_2}{k_{-1}} [1][\text{PyNO}] \quad (3)$$

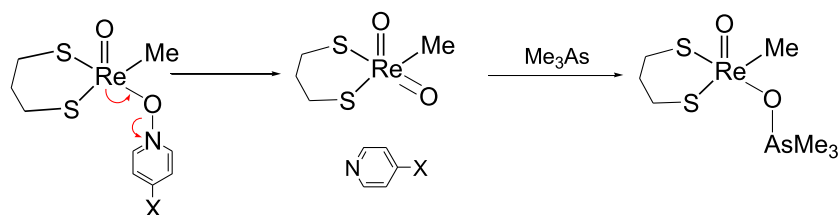
Eq (3) can be simplified to Eq (4).

$$\nu = K_{\text{eq}} K_2 [1][\text{PyNO}] \quad (4)$$

$$\nu = K[1][\text{PyNO}], k = K_{\text{eq}} k_2 \quad (5)$$

3.3. Hammett analysis

The experimental second order rate constants are sensitive to the nature of the substituent on pyridine oxide Me > H > NO₂, with reaction constant $\rho = -1.4 \pm 0.1$ (**Fig. 5**). The reaction constant is estimated from the relative rate constant to the hammett substituent constant (**Table 1**). The second order rate constant (k) depends on the K_{eq} and k_2 values (Eq (5)). The increase in the rate constant can be traced to increase of either K_{eq} or k_2 or both. The electron donor substituent on pyridine oxide increases the rate of reaction. The first equilibrium of the proposed mechanism will be enhanced with more electron donor substituent as more basic ligand will coordinate faster. The second step (oxidation of rhenium and reduction of pyridine oxide) is thought to be inhibited with electron donor substituent on the pyridine oxide because reduction of the pyridine ring will be less favored by electron donor substituent. The



X= Me₂N, MeO, Me, H, Cl, NO₂

Scheme 4. The simplified reaction model for the DFT calculation.

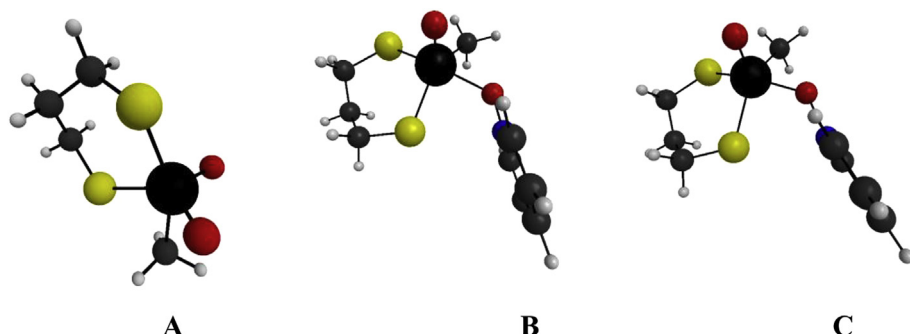


Fig. 6. The DFT optimized structure: A is the Me(pdt)Re^{VII}O₂, B is the optimized structure of Me(pdt)Re^V-OpyN intermediate, C is the transition state structure of the pyridine release and Me(pdt)Re^{VII}O₂ formation.

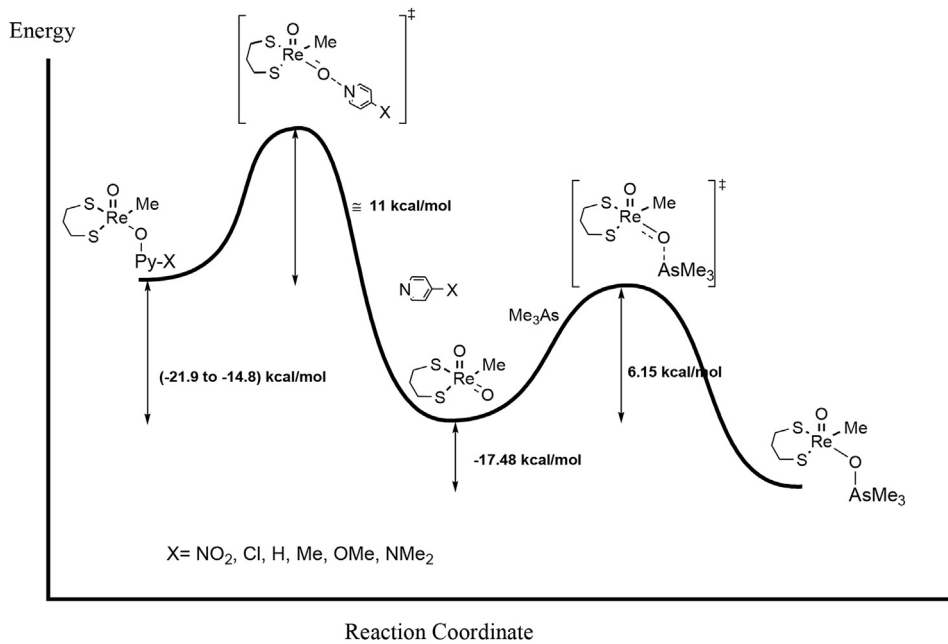


Fig. 7. The DFT calculated reaction coordinate of the simplified model reaction.

Table 2

The enthalpy, entropy, and Gibbs free energy of activation of the proposed slow step with different pyridine oxide substituent and the fast step.

Reaction	ΔH^{\ddagger} (kcal/mol)	ΔS^{\ddagger} cal K ⁻¹ mol ⁻¹	$\Delta G^{\ddagger a}$ (kcal/mol)
	11.5	-0.71	11.66
	11.3	0.167	11.28
	11.6	-0.64	11.79
	11.7	0.39	11.55
	11.2	0.11	10.84
	11.4	0.72	11.19
	6.1	-44.1	19.2

^a At T = 298.15 K; $\Delta G^{\ddagger} = \Delta H^{\ddagger} - T\Delta S^{\ddagger}$

experimental results shows the electron donor substituent increases the reaction rate constant and the electron withdrawing substituent decreases the reaction rate constant. This suggests that the first equilibrium is more affecting by nature of the substituent than the second oxidation step.

3.4. Computational study

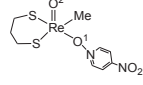
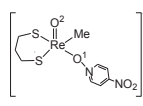
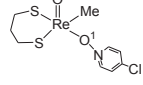
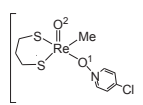
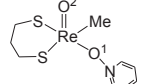
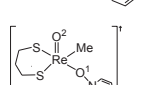
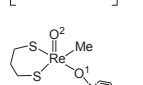
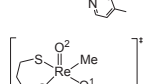
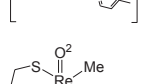
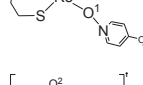
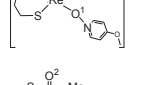
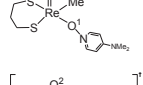
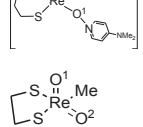
To gain a better understanding on the reaction mechanism and the substituent effect, the DFT calculations have been done on the

rate determining step and the fast step of the reaction as well. Due to the time limitation to run the calculation on the actual catalysis and the reactants, certain simplification has been used in which the Me(pdt)Re^VO-OpyN-X and Me(pdt)Re^{VII}O₂ (**Scheme 3**) are used in place of I₁ and I₂ intermediates in **Scheme 2** and Me₃As is used in place of Ph₃As. This small model of the dimer is valid as the other half of the Re dimer isn't directly involved in the proposed mechanism.

In the kinetics experiments only three substrates have been used because of the starting materials availability. But in the

Table 3

Selected bond lengths (Å) and angles and Mulliken charges on Re, O, and N.

	Re-O ²	Re-O ¹	O ¹ -N	Re-O ¹ -N angle	Charge, Re	Charge, O ¹	Charge, N
	1.68	2.10	1.34	125.4	0.44	-0.53	-0.05
	1.68	1.89	1.62	126.6	0.57	-0.52	-0.21
	1.68	2.08	1.36	123.9	0.44	-0.54	-0.07
	1.68	1.89	1.64	126.2	0.57	-0.52	-0.23
	1.68	2.08	1.36	124.6	0.45	-0.55	-0.07
	1.68	1.88	1.66	126.1	0.58	-0.53	-0.22
	1.68	2.07	1.36	123.5	0.45	-0.55	-0.07
	1.68	1.88	1.66	126.3	0.58	-0.53	-0.23
	1.68	2.06	1.37	124.3	0.46	-0.55	-0.09
	1.68	1.87	1.67	126.3	0.58	-0.52	-0.25
	1.68	2.05	1.37	125.0	0.46	-0.56	-0.10
	1.68	1.87	1.68	126.6	0.59	-0.53	-0.26
	1.69	1.69			0.65	-0.46	

computational study, more substrates were tested to understand the substituents effect (**Scheme 4**). Six substituted pyridine oxide have been used varying from strong electron withdrawing to strong electron donor substituent.

The calculated structure of $\text{Re}^{\text{VII}}\text{O}_2$ key intermediate is a distorted trigonal bipyramidal in which the oxo group occupy the equatorial position (**Fig. 6**, A). This result is consistent with earlier computational studies that showed the dioxo d^0 octahedral complexes form stable *cis*-dioxo complexes [50,51]. The optimized structure of $\text{Me}(\text{pdt})\text{Re}^{\text{V}}\text{O}-\text{OPyN}$ and its transition state structure of pyridine release are illustrated in **Fig. 7** (B and C). The other optimized structure and transition state structure of the substituted pyridine oxide are presented in the **supporting information** along with the coordinates. All the transition states have been verified by the intrinsic reaction coordinate (IRC) calculation on the located transition state.

The activation barrier for $\text{Re}^{\text{VII}}\text{O}_2$ formation and pyridine release were calculated for six pyridine oxide substituents (**Table 2**). The calculated barrier ($\Delta H^{\circ,\ddagger}$) is unaffected by the nature of the substituent on the pyridine oxide and approximately ≈ 11.5 kcal/mol. The average Gibbs free energy of activation ($\Delta G^{\circ,\ddagger}$) is 11.4 kcal/mol and also not affected by the nature of the substituent. The entropy of activations ($\Delta S^{\circ,\ddagger}$) of the slow step are very small and slightly positive except for NO_2 and H substituent are slightly negative. The activation barrier of the fast step (nucleophilic addition of the Me_3As to $\text{Re}^{\text{VII}}\text{O}_2$ step) is 6.15 kcal/mol (**Table 2**) and has large negative entropy of activation which agree with associative nature of the reaction. The activation barrier is lower than the activation barrier of the rate determining step which agree with the experimental finding that the arsine inter the catalytic after the rate determining step. The reaction coordinate has been calculated by DFT for the proposed slow and the fast steps of the mechanism using the above reaction model (**Fig. 7**).

The above results of $\Delta H^{\circ,\ddagger}$ promoted us to examine the $\text{Re}=\text{O}$, $\text{Re}-\text{O}$, and $\text{N}-\text{O}$ bond length of the Re^{V} intermediates and the transition states in addition to mulliken charges on Re^{V} , O, N, and Re^{VII} . **Table 3** summarize our results. In all transition states the $\text{Re}-\text{O}$ length decreases and the $\text{O}-\text{N}$ bond increases as expected. The

mulliken charges on Re increases as results of the oxidation and the negative charges on the N increases as result from the reduction. The charges on the nitrogen doesn't change with substituent even though there are a little increase on the charge with strong electron donor substituent (MeO^- , Me_2N^-). There is small elongation observed on the $\text{N}-\text{O}$ with MeO^- and Me_2N^- substituent compared to others in both transition state and intermediates. The $\text{Re}-\text{O}^1$ are not changed significantly with substituents for both optimized minima and transition state. The substituents on the pyridine oxide don't have any significant changes on the $\text{N}-\text{O}$ and $\text{Re}-\text{O}^1$ bond length and the charges on both N and O^1 which confirm that the rate determining step is not sensitive to the nature of the substituent.

The DFT estimated the thermodynamic parameters of the slow oxidation Re^{V} to Re^{VII} and release of the pyridine step is exothermic and exergonic for all substituted pyridine oxide (**Table 4**). But more negative ΔH° and ΔG° obtained with electron withdrawing group because the reduction of N of the aromatic ring will be more favored with electron withdrawing group.

The computational results explain the zero order dependence on the triphenylarsine but doesn't explain the Hammett dependence. The Hammett analysis shows that the electron donating substituent increase the rate of the reaction. Based on computational results, it can be assume that the Hammett substituent effect came from the first equilibrium step. As basicity of pyridine oxide increases with electron donor substituent, the first equilibrium step will shift to right to form more I_1 (**Scheme 2**) which will increase the reaction rate.

The influence of the substituent on the first equilibrium is not applicable to study computationally because of large time needed to run the calculation on the dimer without simplification. But it can be examined indirectly relative to pyridine according to Eq (3). The ΔH of Eq (3) indicate how the substituent can influence the first equilibrium step compare to pyridine oxide. Since the other rhenium atoms isn't involve in the reaction, it can be studied using a small model of the rhenium dimer (Eq (4)). Eq (4) is an isodesmic reaction in which the error of the computation will be the minimum. **Table 5** summarized our results.

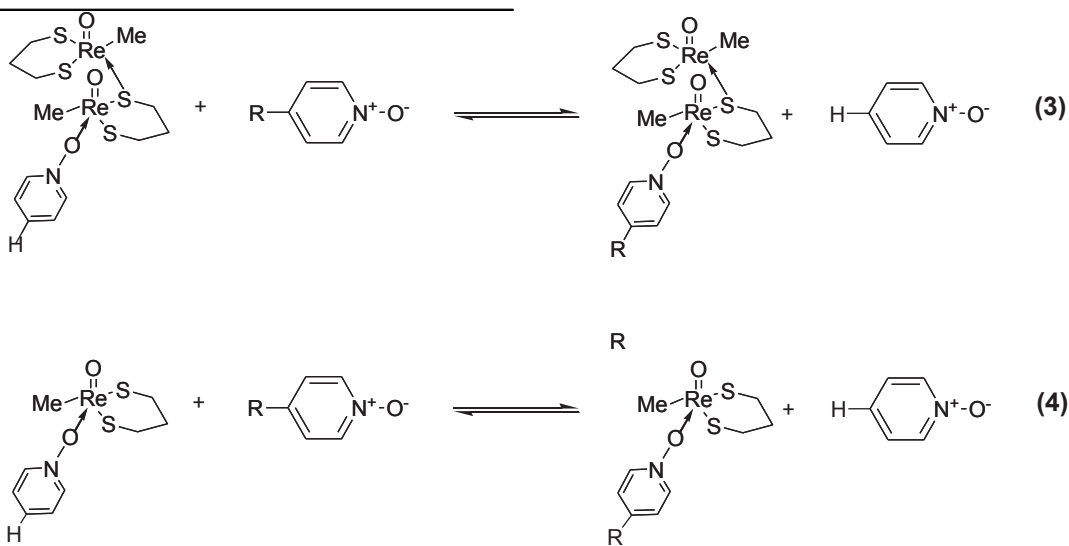
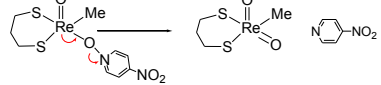
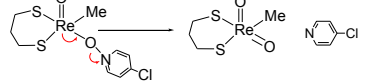
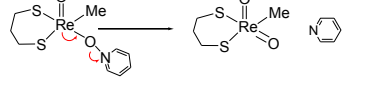
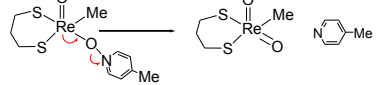
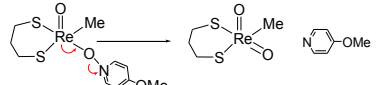
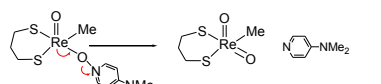
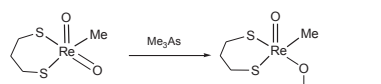


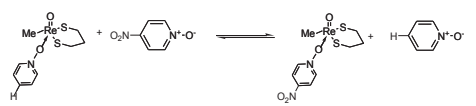
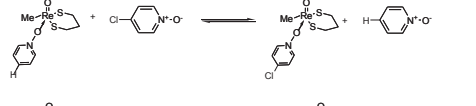
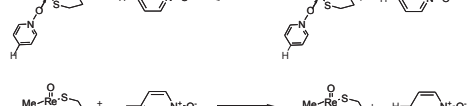
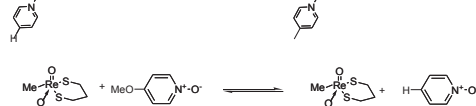
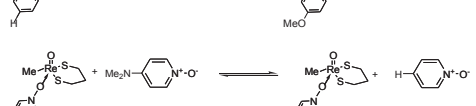
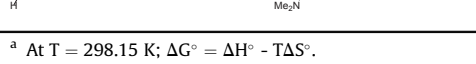
Table 4

The enthalpy, entropy, and the Gibbs free energy of the proposed slow step with different pyridine oxide substituent and the fast step.

Reaction	ΔH° (kcal/mol)	ΔS° cal K ⁻¹ mol ⁻¹	ΔG° ^a (kcal/mol)
	-21.7	46.6	-35.6
	-19.9	45.9	-33.6
	-17.7	44.1	-30.8
	-16.8	46.9	-30.8
	-17.7	47.7	-31.9
	-14.6	46.8	-28.6
	-17.5	-44.8	-4.1

^a At T = 298.15 K; $\Delta G^\circ = \Delta H^\circ - T\Delta S^\circ$.**Table 5**

The enthalpy and Gibbs free energy of reaction 4 with different substituent.

Reaction	ΔH_4° kcal/mol	ΔS_4° cal K ⁻¹ mol ⁻¹	ΔG_4° ^a kcal/mol
	3.80	-2.72	4.61
	0.16	-1.81	0.70
	0.00	0.00	0.00
	-1.73	-1.69	-1.22
	-2.58	-3.39	-1.57
	-5.71	-6.95	-3.64

^a At T = 298.15 K; $\Delta G^\circ = \Delta H^\circ - T\Delta S^\circ$.

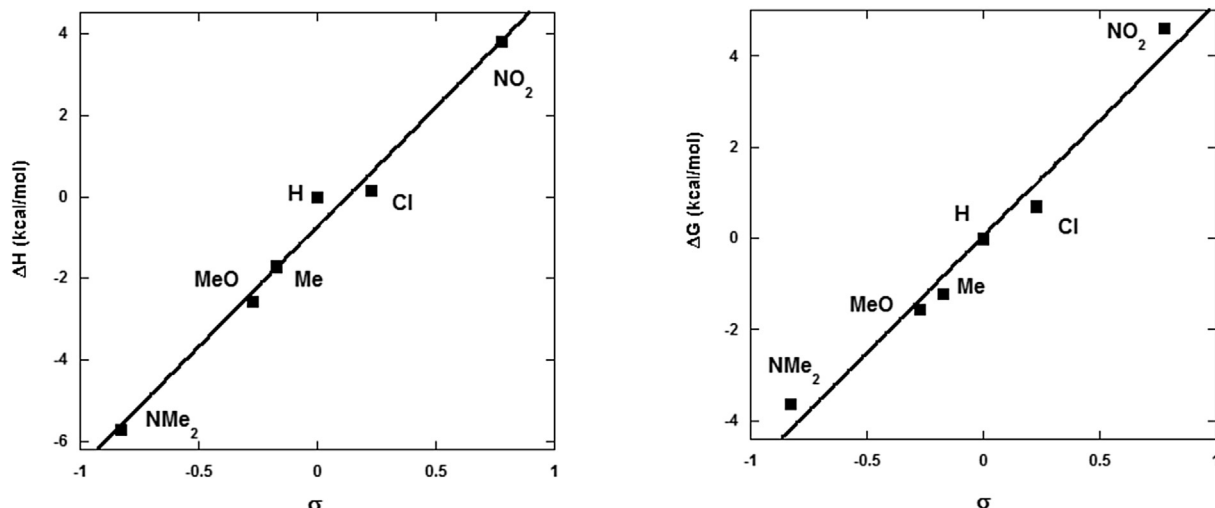


Fig. 8. (Left) Plot of enthalpy of Eq (4) (ΔH_4°) against Hammett (σ) substituent constant, (Right) Plot of ΔG_4° of Eq (4) against Hammett (σ) substituent.

The enthalpy (ΔH_4°) and Gibbs free energy (ΔG_4°) of reaction 4 provides a qualitative analysis how the coordination to rhenium center is influenced by the nature of the substituent on the pyridine oxide. The negative enthalpy and Gibbs free energy of reaction with electron donor substituent (entries 1 and 2) indicates that the rhenium coordinate better with electron donor substituted pyridine oxide and prefer the electron donor substituent compare to pyridine oxide. This will shift the equilibrium (K_{eq}) to right to form more I_1 intermediate (Scheme 2). The positive enthalpy and Gibbs free energy of reaction with electron withdrawing substituent (entries 4, 5 and, 6) indicate that rhenium center coordinate weaker with electron withdrawing substituent. This will shift the equilibrium (K_{eq}) of the proposed mechanism to the left to form less I_1 intermediate. These results agree with experimental finding that NO₂ substituent is slower than pyridine oxide and the methyl substituent is faster than pyridine oxide. Also, there is a good correlation between the enthalpy of Eq (4) (ΔH_4°) and Gibbs free

energy of Eq (4) (ΔG_4°) values with the Hammett (σ) substituent constant (Fig. 8).

3.5. Activation parameters

The second-order rate constant for the pyridine oxide reaction, as defined in Eq (1), was determined at the different temperatures of 15.0, 20.0, 25.0, and 35.0 °C. The data were fit by the transition-state theory equation

$$\ln(k/T) = \ln(k_B/h) + \Delta S^\ddagger/R - \Delta H^\ddagger/RT \quad (6)$$

Fig. 9 displays the plot of $\ln(k/T)$ vs $1/T$ for pyridine oxide. The plots of nitro and methyl substituent are available in supporting information. From slope and the intercept the ΔH^\ddagger in kcal mol⁻¹ and ΔS^\ddagger cal K⁻¹ mol⁻¹ were obtained. Table 6 summarize our results.

The experimental entropy of activation $\Delta S^\ddagger = \Delta S_1^\circ + \Delta S_2^\circ \ddagger$. The ΔS_1° is substantially negative because two molecules associate to one molecule in the first equilibrium. The ΔS_2^\ddagger (estimated in Table 2) are slightly positive for NO₂ and H substituent and slightly negative methyl substituent. The experimental ΔS^\ddagger for the three pyridine oxide substrates are negative means that ΔS_1° is the most anticipating in the total entropy of activation.

The experimental ΔH^\ddagger increases as electron withdrawing substituent attached to pyridine oxide ($\Delta H_{NO_2}^\ddagger > \Delta H_H^\ddagger > \Delta H_{Me}^\ddagger$). These results agree with experimental reaction rate that the picoline *N*-oxide is faster than pyridine *N*-oxide and pyridine *N*-oxide is faster than 4-nitropyridine *N*-oxide. The experimental $\Delta H^\ddagger = \Delta H_1^\circ + \Delta H_2^\ddagger$. The DFT estimated values ΔH_2^\ddagger are 11.7, 11.6, and 11.5 kcal/mol for 4-picoline *N*-oxide, pyridine *N*-oxide, and 4-nitropyridine *N*-oxide, respectively (Table 2). The projected values of ΔH_1° ($\Delta H_1^\circ = \Delta H_{(exp)}^\ddagger - \Delta H_{2(DFT)}^\ddagger$) are 2.7, 0.5, and -1.2 kcal/mol, respectively. The ΔH_1° shows how the thermodynamic of the first equilibrium changed by the nature of the substituent. It is less

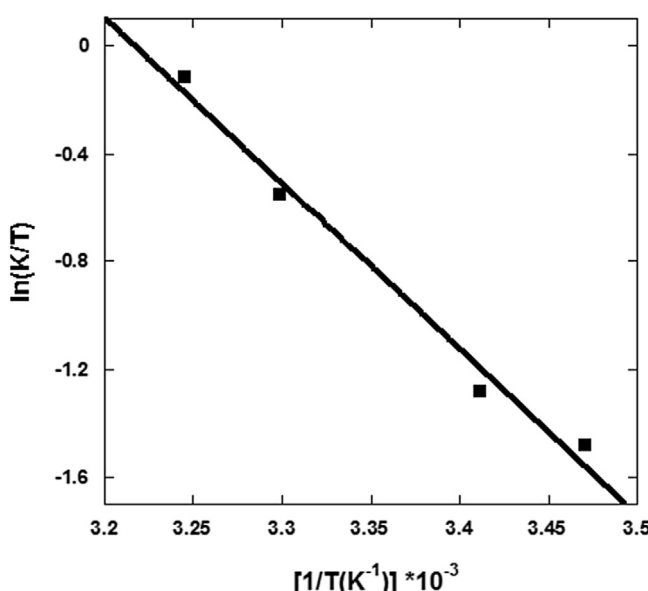


Fig. 9. Plot of $\ln(k/T)$ versus $1/T$ of the pyridine oxide (0.5 mM) reaction with triphenyl arsine (1 mM), and rhenium dimer (0.014 mM).

Table 6
The estimated activation parameters of reaction 1

substrate	ΔH^\ddagger /(kcal/mol)	ΔS^\ddagger (cal/mol.k)
4-nitropyridine <i>N</i> -oxide	14.3 ± 1.0	-10 ± 3
pyridine <i>N</i> -oxide	12.2 ± 1.0	-8 ± 4
4-picoline <i>N</i> -oxide	10.5 ± 0.2	-11 ± 1

favored than pyridine with NO_2 substituent (electron withdrawing substituent). With methyl substituent, the ΔH_1^\ddagger is negative indicating a more favored equilibrium than pyridine to form the I_1 intermediate. The above results agree with experimental the rate increase with electron donating substituent and decrease with electron withdrawing substituent. These values of ΔH_1^\ddagger are estimated based on the experimental values of ΔH_1^\ddagger and the DFT estimated ΔH_2^\ddagger and they reasonably agree with ΔH^\ddagger of Eq (4) (Table 5). Pyridine oxide with electron donor substituent coordinate better with rhenium center to form more of the I_1 intermediate which leads to faster reaction. But pyridine oxide with electron withdrawing group coordinate weaker with rhenium center to form less of I_1 intermediates which leads to slower reaction.

In conclusion, the kinetics and the DFT calculation results shows that the reaction is first order with respect to the pyridine oxide and the catalysis and zero order with respect to the Ph_3As . The pyridine oxide coordinate to one rhenium atom of the catalyst followed by oxidation of Re^{V} to Re^{VII} and release of pyridine (RDS). The Ph_3As inter the catalytic cycle after the rate determining step to reduce Re^{VII} to Re^{V} . The reaction rate is $\rho = -1.4$ means that the reaction rate is sensitive to the nature of the substituent on the pyridine oxide and increases with electron donor substituents. The DFT calculation on the proposed RDS shows that it is unaffected by the nature of the substituent on the pyridine oxide but the first equilibrium step is influenced by the nature of the substituent. The electron donor substituent enrich first step of the proposed mechanism (K_{eq}) which will increase the concentration of the I_1 along with the reaction rate.

Acknowledgments

This work was supported by Jordan University of Science and Technology, Irbid, Jordan (20140257).

Appendix A. Supplementary data

Supplementary data related to this article can be found at <http://dx.doi.org/10.1016/j.jorgchem.2017.04.034>.

References

- [1] R. Hille, J. Hall, P. Basu, The mononuclear molybdenum enzymes, *Chem. Rev.* (Washington, D.C. U.S.) 114 (2014) 3963–4038.
- [2] L.S. Shul'pina, A.R. Kudinov, D. Mandelli, W.A. Carvalho, Y.N. Kozlov, M.M. Vinogradov, N.S. Ikonnikov, G.B. Shul'pin, Oxidation of alkanes and benzene with hydrogen peroxide catalyzed by ferrocene in the presence of acids, *J. Organomet. Chem.* 793 (2015) 217–231.
- [3] L.X. Alvarez, A.B. Sorokin, Mild oxidation of ethane to acetic acid by H_2O_2 catalyzed by supported μ -nitrido diiron phthalocyanines, *J. Organomet. Chem.* 793 (2015) 139–144.
- [4] P. Gonzalez-Navarrete, F.R. Sensato, J. Andres, E. Longo, Oxygen atom transfer reactions from mimoun complexes to sulfides and sulfoxides. A bonding evolution theory analysis, *J. Phys. Chem. A* 118 (2014) 6092–6103.
- [5] Y. Hasenaka, T.-a. Okamura, M. Tatsumi, N. Inazumi, K. Onitsuka, Behavior of anionic molybdenum(IV, VI) and tungsten(IV, VI) complexes containing bulky hydrophobic dithiolate ligands and intramolecular $\text{NH}\cdots\text{S}$ hydrogen bonds in nonpolar solvents, *Dalton Trans.* 43 (2014) 15491–15502.
- [6] H. So, Y.J. Park, K.-B. Cho, Y.-M. Lee, M.S. Seo, J. Cho, R. Sarangi, W. Nam, Spectroscopic Characterization and Reactivity Studies of a mononuclear nonheme Mn(III)-Hydroperoxo complex, *J. Am. Chem. Soc.* 136 (2014) 12229–12232.
- [7] G. Yin, Understanding the oxidative relationships of the metal oxo, hydroxo, and hydroperoxide intermediates with manganese(IV) complexes having bridged cyclams: correlation of the physicochemical properties with reactivity, *Acc. Chem. Res.* 46 (2013) 483–492.
- [8] R. Sarkar, A. Hens, K.K. Rajak, Synthesis, characterization and DFT study of oxorhenium(V) complexes incorporating quinoline based tridentate ligands, *RSC Adv.* 5 (2015) 15084–15095.
- [9] B.K. Panda, U. Senapati, B. Mondal, S. Sengupta, Oxidorhenium(V) and imidorhenium(V) complexes of pyridylpyridazine: oxygen atom transfer, oxidation and substitution involving oxido, phosphine oxide and phosphine coordination, *Chem. Sci. Trans.* 4 (2015) 337–346.
- [10] H. Tang, J. Guan, H. Liu, X. Huang, Comparative insight into electronic properties and reactivities toward C-H bond activation by iron(IV)-nitrido, iron(IV)-oxo, and iron(IV)-sulfido complexes: a theoretical investigation, *Inorg. Chem.* 52 (2013) 2684–2696.
- [11] J.L. Smeltz, C.P. Lilly, P.D. Boyle, E.A. Ison, The electronic nature of terminal oxo ligands in transition-metal complexes: ambiphilic reactivity of oxorhenium species, *J. Am. Chem. Soc.* 135 (2013) 9433–9441.
- [12] A. Ibdah, Computational study on chain pathways for oxygen atom transfer catalyzed by a methyl(dithiolate) thiorhenium(V) compound, *React. Kinet. Mech. Catal.* 116 (2015) 339–350.
- [13] X. Shan, J.H. Espenson, S. Huang, R. Alberto, Methyl(oxo)rhenium(V) complexes with chelating ligands, 30, *Inorg. Synth.* 36 (2014) 155–159.
- [14] G. Du, M.M. Abu-Omar, Oxo and imido complexes of rhenium and molybdenum in catalytic reductions, *Curr. Org. Chem.* 12 (2008) 1185–1198.
- [15] M. Li, A. Ellern, J.H. Espenson, Rhenium(V) complexes with thiolato and dithiolato ligands: synthesis, structures, and monomerization reactions, *Inorg. Chem.* 44 (2005) 3690–3699.
- [16] A. Ibdah, R.M. Al-Zoubi, Mechanistic study on rhenium(V) dimer catalysis for the oxygen atom transfer from pyridine oxide to Ph_3E ($\text{E} = \text{P}, \text{As}$): experiment and computational study, *React. Kinet. Mech. Catal.* 118 (2) (2016) 365–376.
- [17] X. Shan, J.H. Espenson, S. Huang, R. Alberto, Methyl(oxo)rhenium(V) complexes with chelating ligands, *Inorg. Synth.* 36 (2014) 155–159.
- [18] R. Hua, J.-L. Jiang, Recent development of rhenium-catalyzed organic synthesis, *Curr. Org. Synth.* 4 (2007) 151–174.
- [19] S. Das, A. Chakravorty, Oxidorhenium(V) complexes of a family of bipyridine-like ligands including pyridyltriazines and pyrazinyltriazine: oxygen-atom transfer, metal redox and correlations, *Eur. J. Inorg. Chem.* (2006) 2285–2291.
- [20] R. Huang, J.H. Espenson, Mechanistic study of oxygen-transfer reaction catalyzed by an Oxorhenium(V) compound, *Inorg. Chem.* 40 (2001) 994–999.
- [21] C. Zhang, I.A. Guzei, J.H. Espenson, Acidic C-H activation of methyltrioxorhenium(vii): isolation and characterization of two compounds having the novel group $\text{C}_5\text{H}_5\text{N}-\text{CH}_2-\text{ReO}_2$ coordinated to tin(iv), *Organometallics* 19 (2000) 5257–5259.
- [22] S. Stankovic, J.H. Espenson, Oxidative cleavage of N,N-Dimethylhydrazones to ketones with hydrogen peroxide, catalyzed by methyltrioxorhenium(vii), *J. Org. Chem.* 65 (2000) 2218–2221.
- [23] G.S. Owens, J. Arias, M.M. Abu-Omar, Rhenium oxo complexes in catalytic oxidations, *Catal. Today* 55 (2000) 317–363.
- [24] G. Lente, I.A. Guzei, J.H. Espenson, Kinetics and mechanism of the monomerization of a Re(V) dithiolato dimer with monodentate ligands. Electronic and steric effects, *Inorg. Chem.* 39 (2000) 1311–1319.
- [25] J.H. Espenson, D.T.Y. Yiu, Kinetics and mechanisms of reactions of Methyl-dioxorhenium(V) in aqueous solutions: dimer formation and oxygen-atom abstraction reactions, *Inorg. Chem.* 39 (2000) 4113–4118.
- [26] Z. Zhu, J.H. Espenson, Methylrhenium trioxide as a catalyst for oxidations with molecular oxygen and for oxygen transfer, *J. Mol. Catal. A Chem.* 103 (1995) 87–94.
- [27] J.H. Espenson, in: American Chemical Society, 2004, p. INOR-338.
- [28] J.H. Espenson, Oxygen transfer reactions: catalysis by rhenium compounds, *Adv. Inorg. Chem.* 54 (2003) 157–202.
- [29] W. Sun, M. Wang, Y. Zhang, L. Wang, Synthesis of benzofuro[3,2-b]pyridines via palladium-catalyzed dual C-H activation of 3-phenoxypridine 1-oxides, *Org. Lett.* 17 (2015) 426–429.
- [30] B. Zorc, The chemistry of heterocycles structure, reactions, syntheses and applications, *Chem. Biochem. Eng. Q.* 10 (1996) 46.
- [31] T. Eicher, S. Haputmann, H. Suschitzky, The chemistry of heterocycles: structure, reactions, Syntheses and Applications, John Wiley & Sons, 2003.
- [32] G. Hughes, M.R. Bryce, Electron-transporting materials for organic electroluminescent and electrophosphorescent devices, *J. Mater. Chem.* 15 (2005) 94–107.
- [33] S. Donck, E. Gravel, N. Shah, D.V. Jawale, E. Doris, I.N.N. Namboothiri, Deoxygenation of amine N-oxides using gold nanoparticles supported on carbon nanotubes, *RSC Adv.* 5 (2015) 50865–50868.
- [34] N.B. Gowda, G.K. Rao, R.A. Ramakrishna, A chemoselective deoxygenation of N-oxides by sodium borohydride-Raney nickel in water, *Tetrahedron Lett.* 51 (2010) 5690–5693.
- [35] N. Koshino, J.H. Espenson, Kinetics and mechanism of oxygen atom transfer from methyl phenyl sulfoxide to triarylphosphines catalyzed by an Oxorhenium(V) dimer, *Inorg. Chem.* 42 (2003) 5735–5742.
- [36] D.S. Barnes, P.M. Burkinshaw, C.T. Mortimer, Enthalpy of combustion of trifluorylarsine oxide, *Thermochim. Acta* 131 (1988) 107–113.
- [37] M.D.M.C. Ribeiro da Silva, M. Agostinha, R. Matos, M.C. Vaz, L.M.N.B.F. Santos, G. Pilcher, W.E. Acree Jr., J.R. Powell, Enthalpies of combustion of the pyridine N-oxide derivatives: 4-methyl-, 3-cyano-, 4-cyano-, 3-hydroxy-, 2-carboxy-, 4-carboxy-, and 3-methyl-4-nitro, and of the pyridine derivatives: 2-carboxy-, and 4-carboxy-. The dissociation enthalpies of the N-O bonds, *J. Chem. Thermodyn.* 30 (1998) 869–878.
- [38] J.H.S. Espenson, Xiaopeng Wang, Ying Huang, Ruili Lahti, David W. Dixon JaNeille Lente, Gabor Ellern, Arkady Guzei, Ilia A. Synthesis and characterization of stoichiometric and catalytic reactions, *Inorg. Chem.* 41 (2002) 2583–2591.
- [39] M.S. Gordon, M.W. Schmidt, in: Elsevier B.V., 2005, pp. 1167–1189.
- [40] M.W. Schmidt, K.K. Baldridge, J.A. Boatz, S.T. Elbert, M.S. Gordon, J.H. Jensen, S. Koseki, N. Matsunaga, K.A. Nguyen, a. et, General atomic and molecular

- electronic structure system, *J. Comput. Chem.* 14 (1993) 1347–1363.
- [41] K.P. Gable, J.J.J. Juliette, C. Li, S.P. Nolan, Thermochemistry of oxygen atom transfer from Cp^*ReO_3 , *Organometallics* 15 (1996) 5250–5251.
- [42] R. Peverati, D.G. Truhlar, M11-L: a local density functional that provides improved accuracy for electronic structure calculations in chemistry and physics, *J. Phys. Chem. Lett.* 3 (2012) 117–124.
- [43] K. Oesz, J.H. Espenson, A non-radical chain mechanism for oxygen atom transfer with a Thiorhenium(V) catalyst, *Inorg. Chem.* 42 (2003) 8122–8124.
- [44] Y. Wang, J.H. Espenson, Kinetics and mechanism of rhenium-catalyzed oxygen atom transfer from pyridine N-Oxides to phosphines, *Inorg. Chem.* 41 (2002) 2266–2274.
- [45] J.H. Espenson, S.M. Nabavizadeh, Kinetic and equilibrium studies of reactions of N-heterocycles with dimeric and monomeric oxorhenium(V) complexes, *Eur. J. Inorg. Chem.* (2003) 1911–1916.
- [46] F.E. Inscore, H.K. Joshi, A.E. McElhaney, J.H. Enemark, Remote ligand substituent effects on the properties of oxo-Mo(V) centers with a single ene-1,2-dithiolate ligand, *Inorg. Chim. Acta* 331 (2002) 246–256.
- [47] G. Lente, J. Jacob, I.A. Guzei, J.H. Espenson, Kinetics and crystallographic studies of the ligand monomerization of a dithiolato(methyl)(oxo)rhenium(V) dimer, *Inorg. React. Mech. Amst.* 2 (2000) 169–177.
- [48] Y. Cai, A. Ellern, J.H. Espenson, New Oxorhenium(V) compound for catalyzed oxygen atom transfer from picoline N-Oxide to triarylphosphines, *Inorg. Chem.* 44 (2005) 2560–2565.
- [49] M.J. Vasbinder, J.H. Espenson, Nucleophilic assistance in rhenium-catalyzed oxygen atom transfer, *Organometallics* 23 (2004) 3355–3358.
- [50] D.C.T. Brower, L. Joseph, D.M.P. Mingos, Metal dp-ligand p conflicts in octahedral oxo, carbyne, and carbonyl complexes, *J. Am. Chem. Soc.* 109 (1987) 5203–5208.
- [51] K.H. Tatsumi, Roald, Bent cis d0 MoO_{22}^{2+} vs. linear trans d0f0 UO_{22}^{2+} : a significant role for nonvalence 6p orbitals in uranyl, *Inorg. Chem.* 19 (1980) 2656–2658.